PAN POLSKA AKADEMIA NAUK

METROLOGY AND MEASUREMENT SYSTEMS

Index 330930, ISSN 0860-8229

www.metrology.pg.gda.pl

M&MS

PROPERTIES OF A FIBRE OPTIC STRAIN SENSOR IN THE CONFIGURATION OF A MACH-ZEHNDER MODAL INTERFEROMETER WITH A POLARIZATION MAINTAINING PHOTONIC CRYSTAL FIBRE

Cezary Kaczmarek

Lublin University of Technology, Faculty of Electrical Engineering and Computer Science, Nadbystrzycka 38A, 20-619 Lublin, Poland (✉ *c.kaczmarek@pollub.pl*, +48 81 538 4309)

Abstract

The paper presents the properties of a strain sensor, which was made using the micro hole collapse method and operates in the configuration of a Mach-Zehnder modal interferometer with a PM-1550-01 polarization maintaining photonic crystal fibre. The sensor's transfer curve was determined analytically. Its strain sensitivity, determined from measurements, decreases slightly with increasing wavelength and is in a range from -2.01 to -2.23 pm/$\mu\varepsilon$ in the wavelength range 1520–1580 nm. Based on the Fourier analysis of the wavelength spectrum of the constructed sensor, the difference of the group refractive indices of the core and the cladding of the photonic crystal fibre was determined, which are in a range from $7.45 \cdot 10^{-3}$ to $1.01 \cdot 10^{-2}$. The temperature sensitivity of the sensor, determined on the basis of measurements performed in a range from 23 to 60°C, is positive and equals 5.9 pm/K.

Keywords: photonic crystal fibre, modal interferometer, temperature sensitivity.

1. Introduction

Fibre optic modal interferometers, which use the interference of two modes propagating in a single optical fibre, have a number of advantages compared with their two-arm counterparts. The most important ones include a significantly reduced impact of environment changes, simplicity and compactness of their structure. The use of photonic crystal fibres in the structure of modal interferometers radically reduces the impact of ambient temperature changes on their properties. This makes it significantly easier to use such interferometers in fibre optic sensorics.

Many sensors of physical and chemical quantities based on modal interferometers have been designed, in which *photonic crystal fibres* (PCFs) have been used. In these designs, most often interferometers in the Sagnac, *Mach-Zehnder* (MZI) and *Michelson* (MI) configurations have been employed. The Sagnac interferometer with a *polarization maintaining photonic crystal fibre* (PM-PCF) is very often used in the design of sensors of such quantities as strain, force, and pressure [1–5]. Its popularity in fibre optic sensorics results from its many advantages. A drawback is its large size, which limits its use in point measurements. The MZI and MI modal interferometers are produced using *long period gratings* (LPGs) [6], optical fibres with mismatching cores [7], micro-collapses in photonic crystal fibres [7–10], tapered fibres [11], and single-mode

Article history: received on Jan. 05, 2018; accepted on Mar. 10, 2018; available online on Jun. 30, 2018, DOI: 10.24425/119563.

fibres with small core radii [12]. Considering the ease of producing the device, simplicity of its structure, as well as mechanical and thermal stability, among the mentioned MZI and MI modal interferometer designs the ones produced using micro collapses in PCFs are outstanding.

The paper presents the testing results of a strain sensor operating in the configuration of a Mach-Zehnder modal interferometer, in which a polarization maintaining photonic crystal fibre PM-1550-01 manufactured by NKT Photonics was used. The interferometer was produced by fusion splicing, with the splices being made in such a way that the air holes in the spliced region of PCF would collapse. The results of testing the following parameters are presented: the dependence of the sensor strain sensitivity on wavelength and the impact of temperature on the spectral characteristics of the interferometer. The differential, group refractive indices of the fibre core and cladding were determined, based on analysis of the spatial frequency spectrum of the sensor.

2. Properties of strain sensor

Figure 1 shows the setup used for measuring the characteristics of a strain sensor based on an MZ modal interferometer (a), a schematic diagram of its structure (b), and a cross-section of the PCF used in its construction (c).

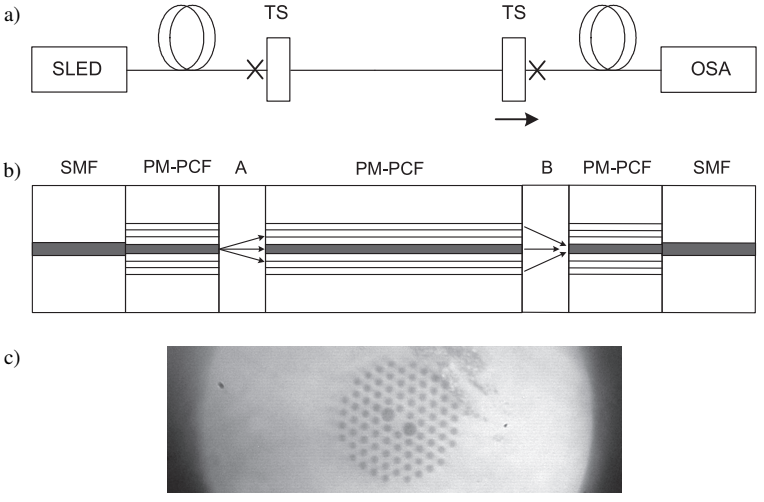

Fig. 1. A test arrangement of the all-PCF modal interferometer (TS-translation stage) (a); a schematic diagram of the interferometer (A, B – collapse regions) (b); a microscope photograph of a PM-PCF cross-section (c).

To build the interferometer of the sensor, a conventional fusion splicer using an electric arc was used, with a designation S183PM, manufactured by Fitel/Furukawa. All splices were performed in the same conditions. First, SMF-28 pigtails were spliced to a prepared segment of the PCF in such a way as to achieve the minimum attenuation at the connections. For this purpose the arc duration and power were reduced compared with those used in splicing standard SMF fibres. The attenuation at the two splices was less than 2 dB. Next, fusion splicing was performed on the PCF in such a way as to cause air holes in the cladding to collapse. The collapses were created at a distance of 150 μm from the splices joining the SMF and the PM-PCF. The total losses of the

sensor's structure are not greater than 6 dB. They seem to depend on the wavelength very little, if at all. The losses affect the amplitude of the sensor's spectrum. However, the output signal of the sensor is a shift of its spectrum, which is not affected by the attenuation.

The phase difference between x and y polarization modes of the core and the excited cladding modes in the photonic crystal fibre of the sensor is defined by the relationship:

$$\Delta\varphi^{ij} = 2\pi \cdot \Delta n^{ij} \cdot L/\lambda, \tag{1}$$

where L, λ, and Δn^{ij}denote, respectively, a length of the interferometer, a wavelength, and a difference of the phase refractive indices of the core and the cladding defined by the relationship:

$$\Delta n^{ij} = n^i - n^j, \tag{2}$$

where $i = x, y$ and $j = 1, 2, \ldots$.

A change of the phase difference $d\Delta\varphi^{ij}$ induced by a change of the length dL (that is by the strain $\varepsilon = dL/L$) of the PM-PCF can be written approximately as follows:

$$d\Delta\varphi^{ij} = 2\pi \left(dL \cdot \Delta n^{ij} + L \cdot d\Delta n^{ij}\right), \tag{3}$$

where $d\Delta n^{ij} = dn^i - dn^j$ is a change of the difference of refractive indices of the core and the cladding induced by the elasto-optic effect. Based on this effect, dn^i and dn^j can be expressed in the form of the relationship:

$$dn^i = p_e^i \cdot n^i \cdot \varepsilon, \qquad dn^j = p_e^j \cdot n^j \cdot \varepsilon, \tag{4}$$

where p_e^i and p_e^j are elasto-optic constants of the PCF core and cladding.

The wavelength spectrum of the interferometer is related to the difference of the group refractive indices of the core and the cladding, which is demonstrated by the relationship (5), obtained after differentiating the relationship (1) and making simple transformations:

$$d\Delta\varphi^{ij}/d\lambda = -2\pi \cdot L \cdot \Delta n_G^{ij}/\lambda^2, \tag{5}$$

where $\Delta n_G^{ij} = n_G^i - n_G^j$ denotes a difference of the group refractive indices of the core n_G^i and the cladding n_G^j. After substituting the relationship (4) into (3) and taking into account the relationship linking the change of the spectrum shift with the change of the phase difference $d\xi^{ij} = \Lambda^{ij} \cdot d\Delta\varphi^{ij}/2\pi$, in which Λ^{ij} denotes a period of the dominant components of the wavelength spectrum, the relationship is obtained:

$$d\xi^{ij} = \frac{\Delta n^{ij}}{\Delta n_G^{ij}} \lambda \left[1 + p_e'\right] \cdot \varepsilon, \tag{6}$$

where $p_e' = (p_e^i n^i - p_e^j n^j)/\Delta n^{ij}$ is a constant defining the impact of the strain on the changes of the refractive indices of the core and the cladding. From (6), it is seen that $d\xi^{ij}$ is directly proportional to ε, therefore a change of the strain of the sensor's fibre will induce a linear shift of its spectrum.

The difference of the group refractive indices of the core and the cladding is defined by the relationship:

$$\Delta n_G^{ij} = \frac{\lambda^2}{L \cdot \Lambda^{ij}} = \frac{\lambda^2 \cdot \zeta^{ij}}{L}, \tag{7}$$

where Λ^{ij} denotes a period of the dominant components of the wavelength spectrum and $\zeta^{ij} = 1/\Lambda^{ij}$ denotes a spatial frequency of the dominant components of the wavelength spectrum. If the interferometer spectrum contains more than one dominant component, it means that excitations of higher order modes in the cladding exist, besides of the one of the first mode. It is easier to determine their spatial frequency than their period. Therefore, the Fourier transformation of the measured wavelength spectrum is performed.

Sensors with the following lengths were used in the tests: 73, 92, 187, 210, and 272 mm. The sensors' characteristics were measured using the setup shown in Fig. 1. The SLED used in the setup had an optical power of 2 mW, a central wavelength of 1562 nm and a spectral width (FWHM) of 40 nm. To determine the strain sensitivity of the sensor, the ends of its fibre were fixed to two precise translation stages. They were used to strain the fibre by applying a series of constant values of strain, while measuring the shift of a selected minimum of the sensor's wavelength spectrum. The strain was applied in a range 0–2.2 mε. The results of these measurements for the sensor with a length of 187 mm and the minimum of the spectrum at a wavelength of 1558.8 nm are shown in Fig. 2. The choice of the particular sensor for measurements had practical reasons. A regular shape of the spectrum and its small period made it easier to measure the wavelength corresponding to the selected minimum of the spectrum. The strain of the sensor's fibre induces a linear shift of its spectrum $d\xi^{x1}$, which is consistent with the relationship (6). The slope of the straight line fitted to the obtained measurement results is the strain sensitivity of the sensor $k_{s\varepsilon} = d\xi^{x1}/d\varepsilon$. The value of this sensitivity is $k_{s\varepsilon} = 2.14$ nm/mε. Its absolute value is approximately two times higher than the strain sensitivity of sensors in the configuration of a Sagnac interferometer with the same PM-PCF [5] and that of uniform *fibre Bragg gratings* (FBG) [13], which do, however, make it possible to reconstruct the strain distribution [14].

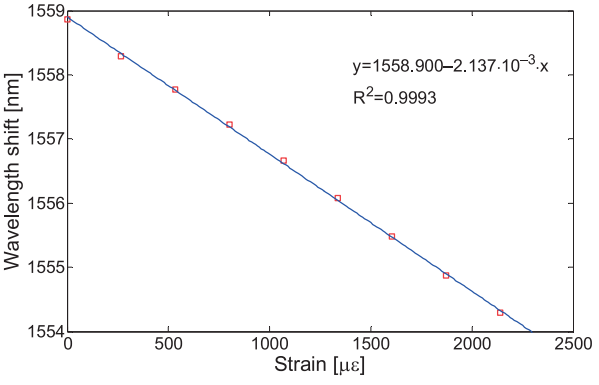

Fig. 2. A shift of the minimum of wavelength spectrum at 1558.8 nm for the sensor with a length of 187 mm as a function of strain.

The results of measurements of sensitivity $k_{s\varepsilon}$ of the tested sensor as a function of wavelength are shown in Fig. 3. From it, it is seen that the strain sensitivity value slightly decreases with increasing wavelength. The dependence of the strain sensitivity on the wavelength results from the dependence on the wavelength of the refractive indices of the core and the cladding of the fibre, which affect the strain sensitivity (6).

In order to determine the temperature sensitivity of the sensor, its temperature was increased in a range 23–60°C and the shift of a selected minimum of its transmission spectrum was measured. A calibration oven was used to heat the sensor. The oven made it possible to set and

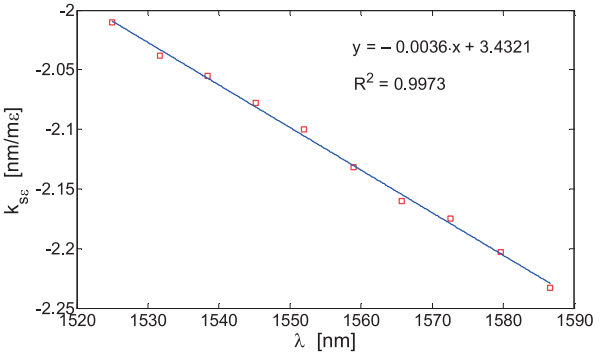

Fig. 3. A spectral strain sensitivity of the sensor as a function of wavelength

maintain the sensor temperature with an accuracy of ± 1°C in a range from the room temperature to 70°C. The results of measurements of the sensor with a length $L = 187$ mm at the wavelength spectrum's minimum of 1559.52 nm are shown in Fig. 4. The temperature sensitivity of the sensor is $k_{sT} = d\xi^{x1}/dT = 5.89$ pm/K. The ratio of the strain sensitivity to the temperature sensitivity of the sensor at a wavelength of 1560 nm is $k_{s\varepsilon}/k_{sT} = 340$ K/nm and has approximately the same value as the same ratio for a strain sensor in the configuration of a Sagnac interferometer with the same PM-PCF, but it is over 3 times smaller than that for an FBG [13]. The sensor can therefore be used to measure strain in a range of mε, while neglecting the effect of temperature, when the changes of ambient temperature are small. When the ambient temperature changes are great, it is imperative to use temperature compensation. This can be achieved by employing the property of the sensor that its strain sensitivity is different for two different wavelengths. When the sensitivities of the sensor are known, it is possible to determine the strain and temperature values from the transfer functions of the sensor based on the measurements of the shift of the spectrum [13]. Another way would be to use a second sensor – passive or active – installed on the measured object for temperature compensation together with the main sensor.

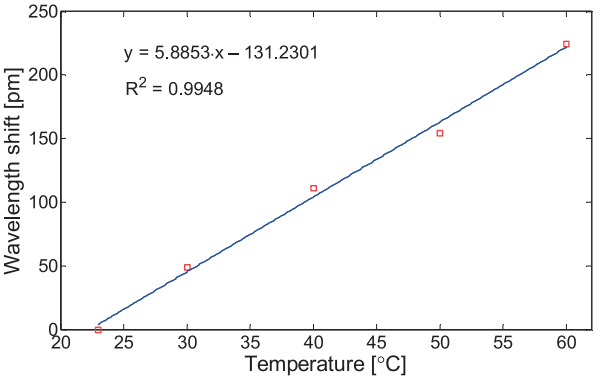

Fig. 4. A shift of the minimum of wavelength spectrum at 1559.52 nm for the sensor with a length of 187 mm as a function of temperature.

To determine the difference between the group refractive indices of the core and the cladding of the fibre, the transmission spectrum was measured for each length of the sensor. Due to the fact

that the SLED has a Gaussian shape of the spectrum, the spectra of the produced interferometers were numerically corrected. This operation was performed based on the measured spectrum of the employed SLED. In order to normalize and better visualize the spectra of sensors of different lengths, the DC component was removed from the original raw spectra. Its value exceeds the spectrum amplitude. By performing the Fourier transformation of the normalized wavelength spectrum, the spatial frequency spectrum of the interference fringes is obtained. The obtained transmission and spatial frequency spectra are shown in Fig. 5. It can be seen that the amplitude of the spectrum slightly decreases with increasing wavelength and that the spatial frequency spectrum contains one dominant component for each length of the interferometer. The observed higher components have a small amplitude. Excitation of several higher order cladding modes was observed in this kind of interferometer when the collapses were longer [7].

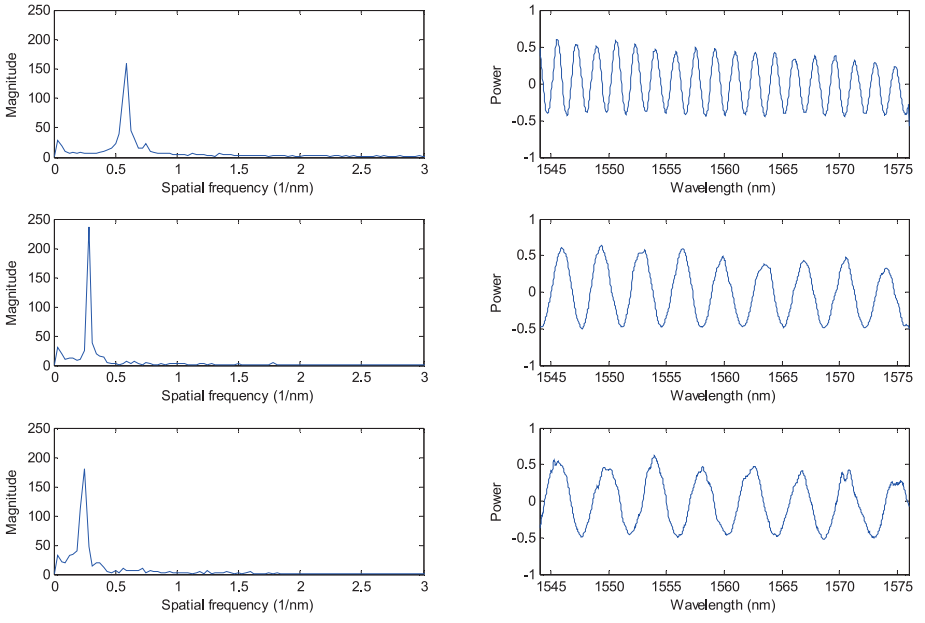

Fig. 5. Normalized transmission spectra of the sensors with three different lengths and the corresponding spatial frequency spectra. From top to bottom: $L = 187$ mm, $L = 92$ mm, $L = 73$ mm.

The calculated spatial frequency as a function of the sensor length is shown in Fig. 6. In the examined wavelength range, the PM-PCF supports only the fundamental mode with its two polarization components. The range of its single-mode operation extends to 1300 nm. Each straight line was approximated from the points, which represent interference of each of the polarization modes of the core with a cladding mode of the same order. The straight line with the less steep slope, approximating the dominant spatial frequency as a function of the interferometer length, represents interference of the polarization mode with the first-order cladding mode, while the straight line with the steeper slope represents interference of the polarization mode with a higher-order cladding mode. Using the slope of the straight line of the dominant spatial frequencies, the difference of the group refractive indices was calculated as $\Delta n_G^{x1} = 7.45 \cdot 10^{-3}$. The other straight line yields $\Delta n_G^{x2} = 1.01 \cdot 10^{-2}$. For the sensor with a length of 272 mm, the difference of the group refractive indices of the core and the cladding determined from (4), based on the measured period of the transmission spectrum at a wavelength of 1560 nm, is $8.4 \cdot 10^{-3}$. This

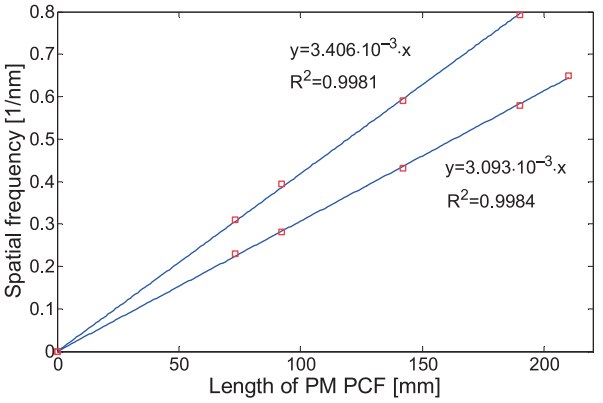

Fig. 6. The calculated dominant spatial frequency as a function of length of the sensor. The two straight lines represent interference of the core mode with two different cladding modes.

means that the observed transmission spectrum of this sensor is a result of interference of the *y* polarization mode with the first cladding mode, if one takes into account the results of analogous calculations for the sensors of different lengths and the fact that the group modal birefringence of the employed PM-PCF is negative. Therefore, $\Delta n_G^{y1} = 8.4 \cdot 10^{-3}$. On this basis it is found that the observed spectra of the sensors, whose lengths are less than 210 mm, are an effect of interference of the *x* polarization mode with cladding modes.

3. Conclusions

From the performed examinations of the sensor, it follows that its strain sensitivity value slightly decreases (the absolute value increases) with increasing wavelength and is in a range from -2.01 to -2.23 pm/$\mu\varepsilon$·m in a wavelength range 1520–1580 nm. The temperature sensitivity value of the sensor measured in a temperature range 23–60°C is 5.9 pm/K. From the performed Fourier analysis of the transmission spectra of the sensors with different lengths, it follows that they contain one dominant component and a very small higher-order component. It indicates the excitation of a weakly attenuated first-order cladding mode in the fibre and a strongly attenuated second-order cladding mode. The differences of the group refractive indices determined based on this analysis are in a range from $7.63 \cdot 10^{-3}$ to $1.01 \cdot 10^{-2}$. The proposed strain sensor can be used for measurements of strain in a range of mε without temperature compensation when the changes of ambient temperature are small. In the case of great ambient temperature changes it is necessary to use temperature compensation, either utilizing the properties of the sensor or employing other, external compensation methods.

References

[1] Dong, X., Tam, H.Y. (2007). Temperature-insensitive strain sensor with polarization-maintaining photonic crystal fiber based Sagnac interferometer. *Appl. Phys. Lett.*, 90(15), 151113–151115.

[2] Kaczmarek, C., Wójcik, W. (2015). Measurement of pressure sensitivity of modal birefringence of birefringent optical fibers using a Sagnac interferometer. *Opt. Appl.*, 45(1), 5–14.

[3] Noh, T.K., Ryu, U.C., Lee, Y.W. (2014). Compact and wide range polarimetric strain sensor based on polarization-maintaining photonic crystal fiber. *Sensors and Actuarors A: Physical*, 213, 89–93.

[4] Gu, B., Yuan, W., He, S., Bang, O. (2012). Temperature compensated strain sensor based on cascaded interferometers and all-solid birefringent hybrid photonic crystal fibers. *IEEE Sensors J.*, 12(6), 1641–1646.

[5] Kaczmarek, C. (2012). Fiber optic strain sensor based on the Sagnac interferometer with a birefringent photonic crystal fiber. *Przegląd Elektrotechniczny*, 88(11b), 288–290.

[6] Lim, J.H., Jang, H.S., Lee, K.S., Kim, C.J., Lee, B.H. (2004). Mach-Zhender interferometer formed in a photonic crystal fiber based on a pair of long-period fiber gratings. *Opt. Lett*., 29(4), 346–348.

[7] Choi, H.Y., Kim, M.J., Lee, B.H. (2007). All-fiber Mach-Zehnder type interferometers formed in photonic crystal fiber. *Opt. Express*, 15(9), 5711–5719.

[8] Villatoro, J., Kreuzer, M.P., Jha, R., Minkovich, V.P., Finazzi, V., Badenes, G., Pruneri, V. (2009). Photonic crystal fiber interferometer for chemical vapor detection with high sensitivity. *Opt. Express*, 17(3), 1447–1453.

[9] Aref, S.H., *et al.* (2009). Modal interferometer based on hollow-core photonic crystal fiber for strain and temperature measurement. *Opt. Express*, 17(21), 18669–18675.

[10] Kaczmarek, C. (2014). Compact PCF modal interferometer for sensor applications built by splicing. *Proc. SPIE 9228*, *Optical Fibers and Their Applications*, 92280R.

[11] Villatoro, J., Minkovich, V.P., Monzon-Hernandez, D. (2006). Compact modal interferometer build with tapered microstructured optical fiber. *IEEE Photon. Technol. Lett*., 18(11), 1258–1260.

[12] Wang, J.N., Tang, J.L. (2012). Photonic crystal fiber Mach-Zehnder interferometer for refractive index sensing. *Sensors*, 12, 2983–2995.

[13] Rao, Y.J. (1997). In-fibre Bragg grating sensors. *Meas. Sci. Technol*., 8, 355–375.

[14] Detka, M., (2017). Response of a uniform optical fiber Bragg grating to strain with a non-smooth distribution: measurements and simulation. *Proc. SPIE 10445, Photonics Applications in Astronomy, Communications, Industry, and High-Energy Physics*, 1044506.